Effects of a Paracyclophane Linker on the Charge-Transfer Transition of 4-(Dimethylamino)-4′-nitrostilbene

Andrew M. Moran,[§] Glenn P. Bartholomew,[†] Guillermo C. Bazan,[†] and Anne Myers Kelley*[,‡]

Department of Chemistry, Kansas State University, Manhattan, Kansas 66506-3701, and Department of Chemistry and Materials, University of California, Santa Barbara, California 93106

Received: January 4, 2002; In Final Form: March 7, 2002

Resonance Raman intensities of the push−pull chromophore 4-(dimethylamino)-4′-nitrostilbene (DANS) have been measured in dichloromethane, acetonitrile, and methanol at excitation wavelengths spanning its strong visible charge-transfer absorption band. The effects of inserting a paracyclophane moiety between the donor and the acceptor are investigated by performing similar measurements on a second molecule, PCP−DANS, which consists of *p*-dihexylaminostilbene and *p*-nitrostilbene moieties attached through their unsubstituted rings by a paracyclophane linker. The Raman excitation profiles and absorption spectra are simulated using time-dependent wave packet propagation techniques to determine reorganization energies along the Raman-active normal coordinates. Excitation to the nominal charge-transfer state generates a much greater change in geometry in the vicinity of the nitro acceptor group in DANS than in PCP−DANS, while the geometry changes around the dialkylamino donor end are similar. Comparison with other push−pull chromophores coupled with the results of ZINDO electronic structure calculations both suggest that the transition in DANS is well-described as an intramolecular charge-transfer transition, whereas the transition in PCP−DANS has less charge-transfer character.

I. Introduction

Push−pull chromophores are characterized by the conjugated linkage of an electron-donating group and an electron-accepting group (see Figure 1). Such molecules are potentially useful for nonlinear optical applications because of large first and second hyperpolarizabilities.[1−12] Molecular design strategies seek to optimize nonlinear polarizabilities by altering the acceptor, donor, and/or conjugated linker. A less common approach involves the insertion of a nonconjugated linker between the acceptor and donor. This approach may be advantageous in terms of both thermal stability and the nonlinearity versus transparency relation.[11]

Inclusion of a paracyclophane (PCP) linker group has been suggested as a viable method of optical property modulation for molecules exhibiting an intramolecular charge-transfer (ICT) transition. The electronic interaction within the PCP moiety results from the stacking of two aromatic rings that are separated by 2.6 Å.[11] In donor−acceptor substituted molecules, ICT involves inter-ring $\pi-\pi$ interactions. The transfer of charge across such a molecule can be viewed in terms of a particle confined within a one-dimensional box with a double potential well. The donor and acceptor groups provide a bias that reduces the energy barrier, inhibiting tunneling from the donor to the acceptor relative to that for an analogous structure without donor and acceptor substitution.[11]

In this work, the effect of a PCP linker on the coupling of molecular vibrations to an ICT-like transition is investigated via resonance Raman intensity analysis. These methods have already been applied to several other molecules exhibiting ICT transitions.[13−20] The important difference between the two compounds studied here involves the presence or absence of PCP in the conjugated pathway between the donor and acceptor groups. The molecules also involve different substituents on the amino nitrogen, although this is assumed to have little effect on the ICT transition characteristics.

II. Experimental and Computational Methods

4-(4′-Dihexylaminostyryl)-16-(4′′-nitrostyryl)[2.2]-paracyclophane (PCP−DANS; see Figure 2) was synthesized using the methods described in ref 11. Solutions of PCP−DANS were prepared in chloroform and acetonitrile (Fisher certified, spectroscopic, or HPLC grades). The molar extinction coefficient for the charge-transfer transition of PCP−DANS in acetonitrile was measured relative to that previously determined in chloroform (54 000 M cm^{-1} at 380 nm) by obtaining spectra of equal dilutions of a common stock solution into each of the solvents. Similarly, solutions of 4-(dimethylamino)-4′-nitrostilbene (DANS) (Kodak) were prepared in methanol, acetonitrile, and dichloromethane (Fisher certified, spectroscopic, or HPLC grades). The molar extinction coefficient for the charge-transfer transition of DANS was measured directly in acetonitrile (26 600 M cm^{-1} at 429 nm). Molar extinction coefficients for the charge-transfer transitions in the other two solvents were determined relative to that in acetonitrile. All absorption spectra were measured on a Hitachi U-3010 UV−visible spectrophotometer. The molar extinction coefficient ϵ (L mol^{-1} cm^{-1}) is related to the absorption cross section σ_A (Å^2 $molecule^{-1}$) by $\sigma_A = 10^{19} \ln(10)\epsilon/N_A$ where N_A is Avogadro's number.

DANS was highly crystalline in the solid state and believed to be almost entirely in the trans configuration, although the isomeric purity of the commercial sample was not stated. The quantum yield for trans → cis photoisomerization in polar

* To whom correspondence should be addressed. Electronic mail: amkelley@ksu.edu.
† University of California, Santa Barbara.
‡ Kansas State University.
§ Current address: Department of Chemistry, University of Rochester, Rochester, NY 14627-0216.

10.1021/jp025504t CCC: $22.00
Published on Web 04/19/2002

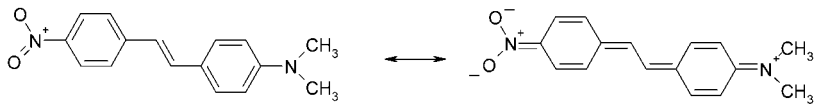

Figure 1. Neutral and zwitterionic structures of DANS.

solvents is less than 0.01,[21,22] and absorption spectra taken before and after the resonance Raman experiments were indistinguishable. The PCP−DANS sample is also assumed to have the stilbene moieties in the trans configuration on the basis of X-ray studies of the compound lacking the electron donor and acceptor groups,[23] and again, no time-dependent changes in the spectra were observed when using acetonitrile as the solvent.

Resonance Raman spectra of PCP−DANS were acquired using the 355 nm third harmonic of a Q-switched Nd:YAG laser (Spectra-Physics GCR 150-30, 30 Hz) and its second and third harmonics Raman-shifted in hydrogen or deuterium to produce the excitation wavelengths 325, 360, 369, 404, and 416 nm. Excitation at 340 nm was generated from a Nd:YAG-pumped, frequency-doubled dye laser (Quantel 6615-10/Lambda Physik F6 3002, 10 Hz) operating with pyridine 1. The excitation wavelengths 390, 429, and 445 nm were provided by a frequency-doubled picosecond mode-locked Ti:sapphire laser (Spectra-Physics Tsunami). Resonance Raman spectra of DANS were acquired using the 390, 404, 429, and 445 nm excitations as well as the 457.9, 465.8, 472.7, 476.5, 488.0, 496.5, 501.7, and 514.5 nm lines from a CW argon ion laser (Lexel model 95-4). For pulsed excitation (wavelengths shorter than 420 nm), the incident beam of ∼0.1 mW at the sample was focused onto a 1 cm fused-silica cell containing about 2 mL of sample solution. The samples were magnetically stirred to protect against thermal or photochemical degradation. For CW excitation (wavelengths longer than 420 nm), the incident beam of 2−5 mW was focused onto about 2 mL of sample contained in a rotating quartz cell. Solutions of PCP−DANS were prepared in the 100−200 μM range, and solutions of DANS ranged from 100 to 500 μM. The actual concentrations were determined spectrophotometrically.

Two different detection systems were used to cover the range of wavelengths employed. For excitation at wavelengths longer than 420 nm, the Raman scattering was collected in a backscattering geometry with aluminum-coated ellipsoidal and flat mirrors and passed through a polarization scrambler before being dispersed by a Spex 1877 triple spectrograph and detected with a Spex Spectrum One liquid nitrogen cooled CCD detector. The slit width at the entrance to the spectrograph stage was 100 μm, giving a spectral resolution of about 6−8 cm^{-1}, depending on the excitation wavelength, for the argon ion excited spectra. The resolution of the Ti:sapphire-excited spectra was lower (11−14 cm^{-1}) because of the greater spectral width of the picosecond pulses. At each setting of the spectrograph, 8 to 20 accumulations of 0.3−2 min each were added. For excitation wavelengths shorter than 420 nm, the Raman scattering was collected in a backscattering geometry with aluminum-coated ellipsoidal and flat mirrors and passed through a polarization scrambler before being dispersed by a SPEX 1702 single spectrograph equipped with a 1200 g/mm grating blazed at 300 nm. The Raman scattering was detected with a Princeton Instruments IRY-700N intensified diode array detector. The slit width was 100 μm, which, convolved with the 3−4 pixel limiting resolution of the intensified detector, yields a spectral resolution of about 7−11 cm^{-1}, depending on the excitation wavelength. At each setting of the spectrograph, 5 to 10 accumulations of 3−5 min each were added and an equivalent number of dark scans subtracted.

The calibration of the frequency axis was accomplished using known solvent lines. Intensities were corrected for the wavelength dependence of the collection and detection systems using an Optronic Laboratories 245C tungsten−halogen lamp.[24] The spectra were further corrected for reabsorption, as described elsewhere for a backscattering geometry.[25] Band areas were determined using the GRAMS/32 (Galactic Industries) curve-fitting algorithm to fit mixed Gaussian−Lorentzian peak profiles. Differential cross sections ($d\sigma_R/d\Omega$) for both DANS and PCP−DANS were calculated relative to known cross sections for selected solvent lines (dichloromethane 702 cm^{-1}, acetonitrile 919 cm^{-1}, and methanol 1035 cm^{-1}).[13,14] Estimated uncertainties in the absolute Raman cross sections are ±15% for the stronger lines.

The resonance Raman intensities and absorption spectra were modeled using the time-dependent formalism described in detail elsewhere.[15,24,26] Each of the modes that has significant intensity on resonance was modeled as a pair of harmonic surfaces with equal ground- and excited-state frequencies and potential minima displaced by a distance Δ in dimensionless normal coordinates. Neither excited-state frequency changes nor the vibrational coordinate dependence of the transition dipole moment (non-Condon effects) were included, as they were not required to obtain good fits to the data. The solvent was modeled as a single Brownian oscillator in the overdamped limit.[27,28] Static inhomogeneous broadening was also included as a Gaussian distribution of zero−zero energies, although the quality of the fits was sensitive to this parameter only for the case of DANS in dichloromethane. As the lowest-frequency mode observed is at 539 cm^{-1}, no thermal population of vibrational levels above the zero-point was considered.

ZINDO[29,30] excitation energies, oscillator strengths, and molecular orbitals were calculated using Gaussian 98 (Gaussian, Inc).[31] The excited states were calculated using configuration interaction among all singly excited configurations formed from 51 occupied and 45 virtual orbitals (DANS) and from 123 occupied and 117 virtual orbitals (PCP−DANS). The DANS geometry was obtained from calculations using the B3LYP hybrid density functional and the 6-311G** basis set. In the case of PCP−DANS, which was too large for DFT calculations, an experimental X-ray structure[23] was used for the core 16 PCP carbon atoms, whereas the remainder of the molecule was optimized with an AM1 semiempirical Hamiltonian.[32] A normal-mode analysis of DANS was performed using the B3LYP hybrid functional and the 6-31G* basis set. Normal modes were viewed with MOLDEN 2.6.

III. Results

A. Absorption Spectra. Figure 3 shows the absorption spectra of DANS in three different solvents. The band shapes and absorption maxima exhibit only a weak solvent dependence within this series, and even a completely nonpolar solvent (cyclohexane) blue-shifts the absorption by only 12 nm relative to that for acetonitrile.[33] Interestingly, small blue-shifts in the absorption maxima are observed in acetonitrile and methanol relative to those in the less polar but highly polarizable dichloromethane. Figure 4 contains the absorption spectra of PCP−DANS in acetonitrile. The absorption maximum of PCP−DANS exhibits even less solvent dependence than that of

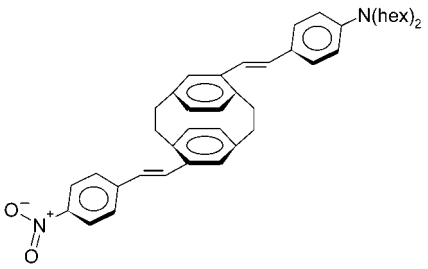

Figure 2. Structure of PCP−DANS.

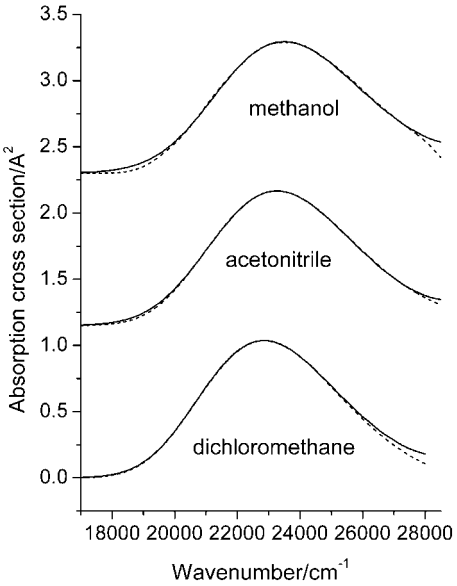

Figure 3. Absorption spectra of DANS in the indicated solvents (solid curves) and spectra calculated from the parameters of Table 1 (dashed curves). Successive spectra are offset vertically by 1.15 Å.

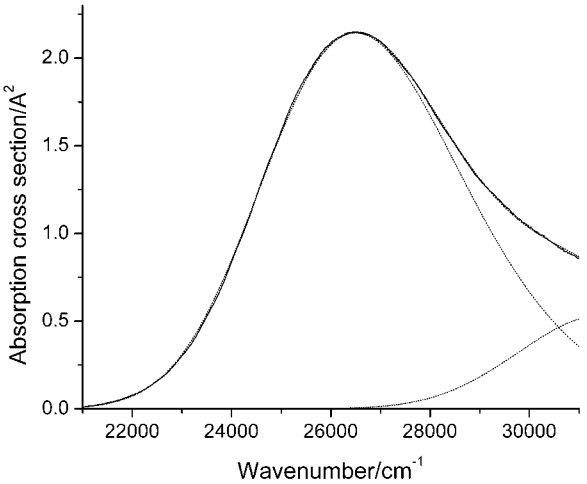

Figure 4. Absorption spectra of PCP−DANS in acetonitrile (solid curve), the individual contributions to the modeled spectrum from the two states (dotted curves), and the sum of the two modeled states (dotted curve nearly indistinguishable from experiment).

DANS, shifting by only 10 nm between nonpolar cyclohexane and extremely polar *N*,*N*-dimethylformamide.[11]

B. Resonance Raman Spectra. Figure 5 presents the Raman spectra of DANS, excited near resonance, in all three solvents. The raw spectra were superimposed on weak fluorescent backgrounds in these solvents, whereas much stronger fluorescence prohibited the experiment from being performed in dioxane. These observations are consistent with previous measurements of the fluorescence quantum yield and Stokes

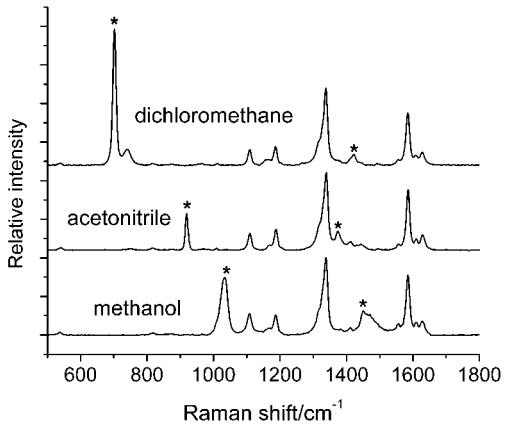

Figure 5. Resonance Raman spectra of DANS in the indicated solvents, excited at 457.9 nm. Weak fluorescence backgrounds have been subtracted. All spectra have been scaled to have approximately equal intensities in the strong 1339 cm^{-1} line. The offsets of the *y*-axes are arbitrary. Asterisks mark lines due primarily to solvent.

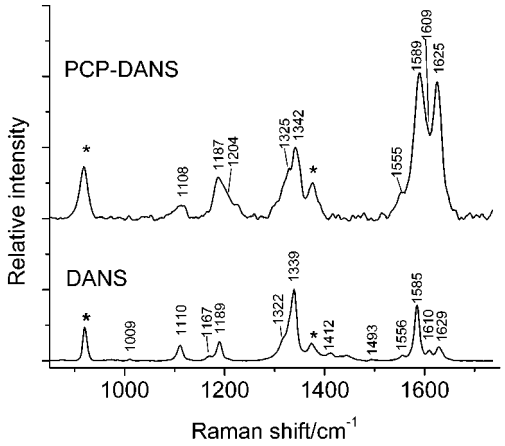

Figure 6. Resonance Raman spectra of DANS and PCP−DANS in acetonitrile. Excitation wavelengths are 457.9 nm for DANS and 390 nm for PCP−DANS. Fluorescence backgrounds have been subtracted. Both spectra have been scaled to have approximately equal intensities in the strong line near 1339 cm^{-1}. The offset of the *y*-axes is arbitrary. Asterisks mark lines due primarily to solvent. The lower resolution of the PCP−DANS spectrum is due primarily to the greater laser bandwidth of the picosecond-pulsed 390-nm radiation compared with that of the CW 457.9-nm line.

shift in multiple solvents.[33−36] The ground-state vibrational frequencies are essentially solvent-independent. Figure 6 compares the Raman spectra of PCP−DANS and DANS excited near resonance in acetonitrile. Similar modes are resonance Raman active in both molecules. Eight of the nine transitions observed in PCP−DANS differ by less than 5 cm^{-1} from corresponding vibrations in DANS. The lowest-frequency line observed in DANS was 539 cm^{-1}, although the spectrum was obtained down to 180 cm^{-1}. The PCP−DANS spectrum was examined down to 400 cm^{-1}, but no transitions with significant intensity were observed below 1108 cm^{-1}.

C. Modeling of Absorption Spectra and Resonance Raman Profiles. For each molecule/solvent pair, the absorption spectrum and resonance Raman excitation profiles were simultaneously fit to a model describing the ground- and excited-state potential energy surfaces. Table 1 contains the fitting parameters, while Figures 3 and 4 and 7−10 show fits to the absorption spectra and excitation profiles, respectively. The classical reorganization energy is defined as the reorganization energy associated with the solvent and any low-frequency molecular modes not explicitly included in the model.

TABLE 1: Spectral Simulation Parameters for DANS and PCP−DANS

	DANS/ dichloromethane	DANS/ methanol	DANS/ acetonitrile	PCP−DANS/ acetonitrile	
electronic inhomog std dev/cm^{-1}	1140	400	0	580	580
electronic homog fwhm (Γ_0)/cm^{-1}	830	1450	2875	3260	3360
electronic line shape param κ	0.1	0.1	0.1	0.1	0.1
classical reorg energy (λ_s)/cm^{-1}	310	947	3725	4789	5087
electronic origin (E_0)/cm^{-1}	19785	19210	17473	21170	26200
transition length/Å	1.996	1.851	1.877	2.418	1.144
refractive index	1.4242	1.3288	1.3442	1.3442	1.3442

	DANS Δ			
DANS vib freq/cm^{-1}	DANS/ dichloromethane	DANS/ methanol	DANS/ acetonitrile	PCP−DANS vib freq/cm^{-1}, Δ
539	0.19	0.564	0.566	
749	*a*	*b*	0.32	
817	0.177	0.398	0.274	
874	*b*	0.208	*b*	
962	0.166	*b*	*b*	
1009	0.127	*b*	0.198	
1110	0.587	0.95	0.584	1108, 0.205
1167	0.572	0.56	0.295	
1188	0.609	0.75	0.55	1187, 0.361 1204, 0.159
1322	0.772	0.978	0.621	1325, 0.221
1339	1.25	1.285	1.005	1342, 0.377
1412	*a*	0.186	0.193	
1494	0.141	*a*	0.123	
1556	0.317	0.298	0.211	1555, 0.323
1585	0.909	0.866	0.89	1589, 0.581
1610	0.284	0.243	0.238	1609, 0.367
1629	0.504	0.401	0.491	1625, 0.513
total vib reorg energy[c] (λ_v)/cm^{-1}	3106	3791	2467	915

[a] Obscured by solvent Raman scattering. [b] Not observed or too weak to be measured accurately in this solvent. [c] Calculated as the sum of $\omega_i\Delta_i^2/2$.

We were unable to simultaneously fit the excitation profiles and the blue side of the absorption spectrum for PCP−DANS with a single electronic transition. It seems clear from examination of the absorption spectrum (see also the more complete spectra in ref 11) that more than one electronic state contributes to the absorption on the high-energy side. ZINDO calculations predict three transitions with significant oscillator strengths ($f = 0.14-0.48$) within 5000 cm^{-1} of the CT transition ($f = 1.09$) of PCP−DANS, whereas a single dominant electronic transition is calculated for DANS in the region of the CT transition. A higher-energy electronic state was therefore added to the PCP−DANS model. The transition dipole moments of the two transitions were assumed to be parallel because the ZINDO transitions with significant oscillator strengths are polarized in roughly the same direction. The normal-mode displacements of this additional state were assumed to be equal to those of the CT state. This assumption is not well justified, but the data do not allow an accurate independent determination of the displacements in the higher-energy state. These assumptions cause the contributions to the Raman amplitude from the two states to interfere destructively in the region to the blue of the lower-energy absorption maximum (above about 26 000 cm^{-1}),[37−39] so that the two-state calculation gives more absorption intensity but less Raman intensity in this region, providing a better fit to most of the Raman profiles. The parameters used to represent the higher-energy state are not very meaningful, and leaving this state out altogether mainly reduces the quality of the fits to the high-energy side of the spectra without much affecting the best-fit parameters. The parameters associated with both states are shown in Table 1.

The complicated multiparametric nature of the spectroscopic modeling makes it difficult to place reliable error limits on the parameters. When all other parameters are held constant, the resonance Raman intensity of each fundamental at each excitation frequency scales approximately as Δ^2; since we choose Δ to best fit the sum of the measured intensities, which is known more accurately than the ±15% uncertainty at each wavelength, the displacements in the individual modes are constrained to considerably better than ±10% if the broadening parameters are held fixed. If we instead fix the normal-mode displacements and vary the two broadening parameters (homogeneous half-width Γ_0 and inhomogeneous standard deviation δ) and the zero−zero energy, we find that the range of broadening parameters that can reasonably fit the absorption spectrum (which has negligible experimental error) and the excitation profiles with their estimated error bars is ±10−20% in both broadening parameters. The actual uncertainties should be considered somewhat larger than this because of coupling between the different parameters; for example, it is possible to decrease the inhomogeneous broadening somewhat further by simultaneously increasing all of the normal-mode displacements (to recover the breadth of the absorption band) and also increasing the homogeneous broadening (adding breadth as well as counteracting the increase in the Raman intensities produced by increasing the displacements). Most of the differences in mode displacements between DANS/dichloromethane and DANS/

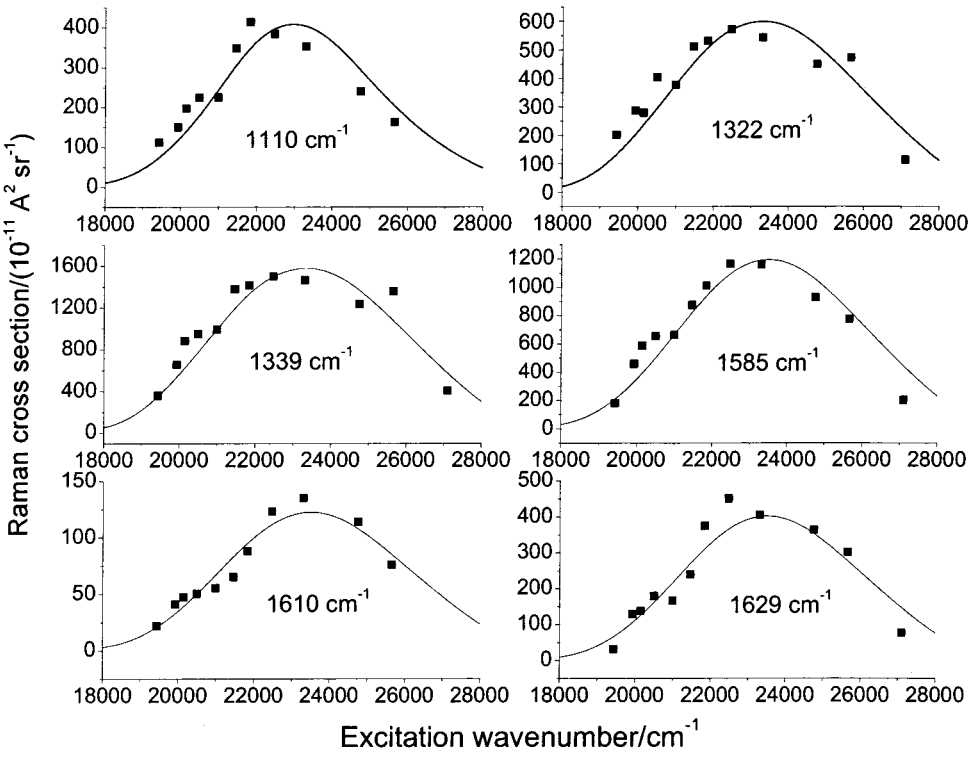

Figure 7. Experimental (points) and calculated (lines) resonance Raman excitation profiles for DANS in dichloromethane. The calculated profiles are generated from the parameters of Table 1.

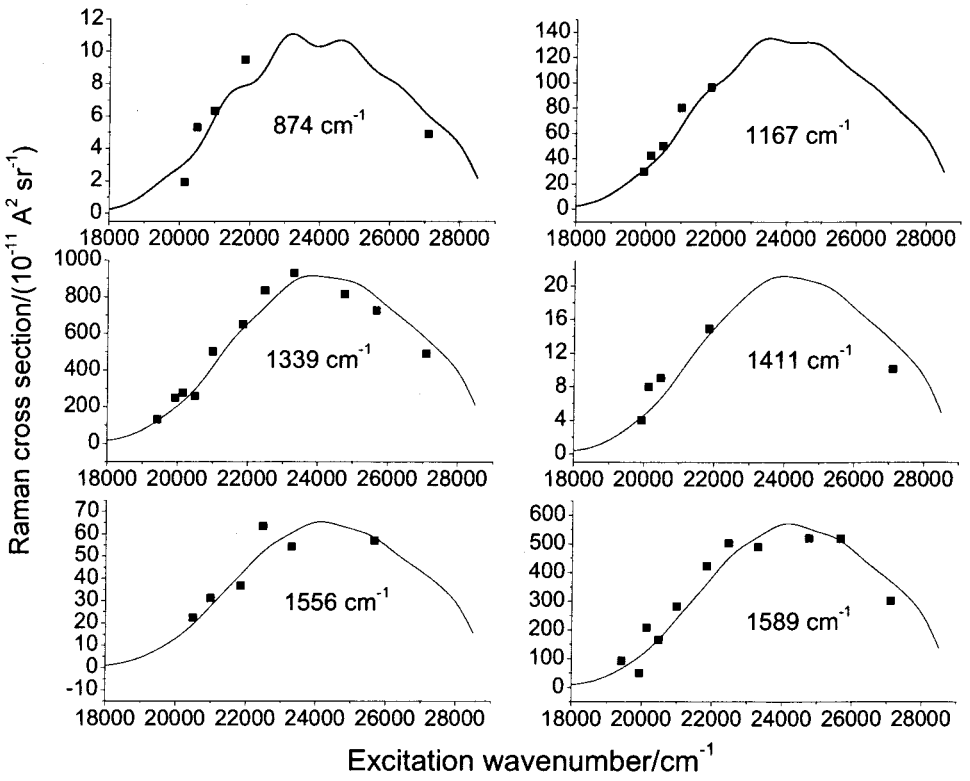

Figure 8. Same as Figure 7 but for DANS in methanol.

methanol should not be considered significant with the exceptions of the 539 and 817 cm^{-1} modes, which while weak are considerably weaker in dichloromethane, and the 1110 cm^{-1} mode, which is anomalously strong in methanol. The smaller Δ values for the 1167, 1188, 1322, 1339, and 1556 cm^{-1} modes in DANS/acetonitrile compared with DANS in the other solvents and for the 1108, 1187, 1325, 1342, and 1589 cm^{-1} modes of PCP−DANS relative to DANS are significant. The differences in homogeneous widths for DANS among the three solvents and the corresponding differences in classical reorganization energy are well outside the uncertainties in the parameters, although the difference in Γ_0 between DANS and PCP−DANS in acetonitrile is not. The differences in inhomogeneous widths among DANS in the three solvents are also well outside the uncertainties in the fitting parameters, although the unusually high value in dichloromethane is hard to rationalize and

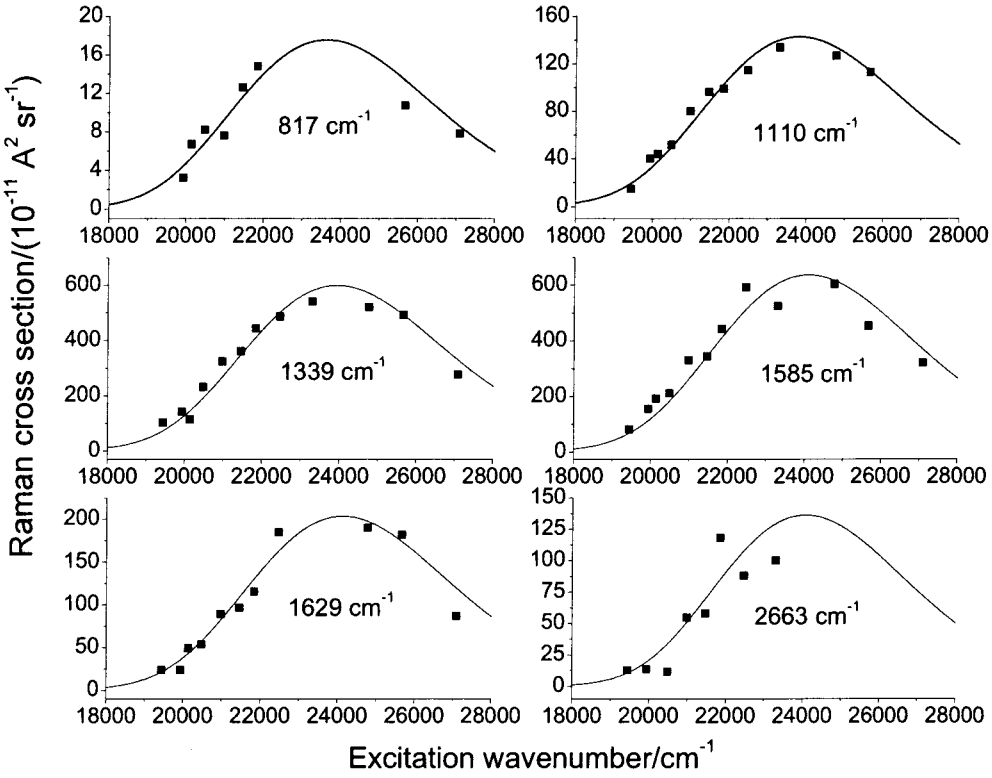

Figure 9. Same as Figure 7 but for DANS in acetonitrile. The 2663 cm^{-1} band contains the overtones of the 1322 and 1339 cm^{-1} modes and the combination band of these two modes.

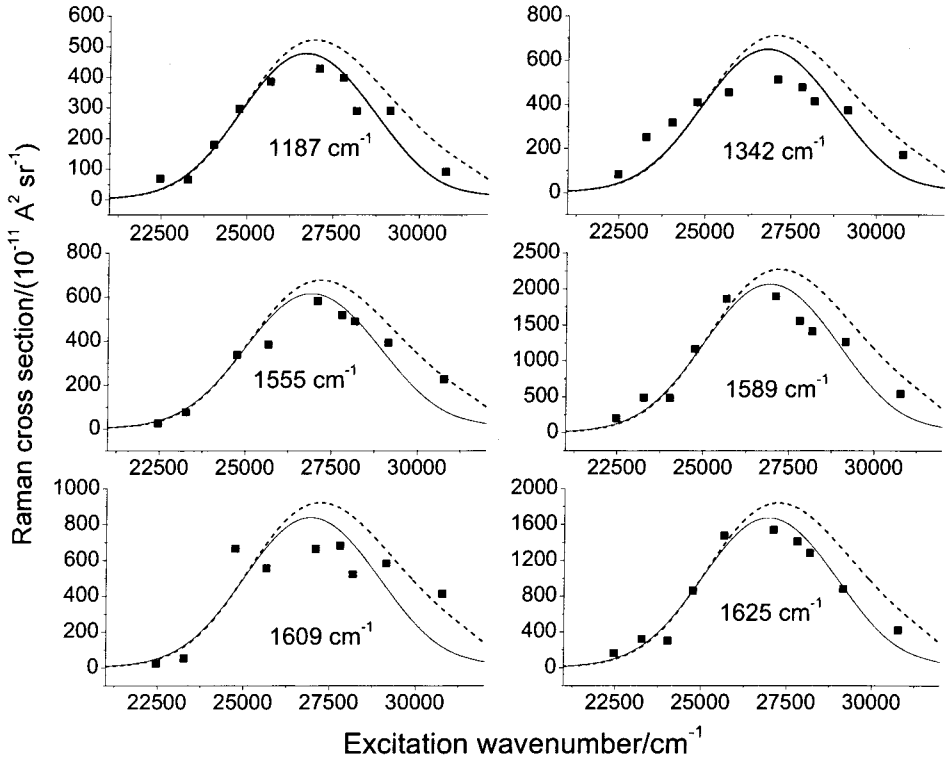

Figure 10. Same as Figure 7 but for PCP−DANS in acetonitrile. The solid and dashed curves represent calculations that include both electronic transitions of Table 1 and only the lower-energy transition, respectively.

inconsistent with the generally small inhomogeneous widths found for other push−pull chromophores in this solvent.[13,14,40]

D. Ground-State Vibrational Modes. Table 2 contains assignments for the vibrational modes of the two molecules. As mentioned above, all but one of the observed modes in PCP−DANS occur within 5 cm^{-1} of a corresponding mode in DANS. Most of the vibrations could be assigned by comparison with previous assignments for the infrared spectrum of DANS[41] and the vibrational spectra of *p*-nitroaniline (PNA),[13] *trans*-stilbene,[42−45] and 4-dimethylaminobenzonitrile (DMABN).[46] The DANS vibrations at 817, 874, 1110, 1322, 1339, 1494, and 1585 cm^{-1} correlate to the NO_2 and ring modes of PNA at 839,

TABLE 2: Vibrational Assignments of DANS and PCP−DANS

DANS expt freq/cm^{-1}	PCP−DANS expt freq/cm^{-1}	DANS expt IR freq, intensity (qual)[a]	DANS calc IR intensity (km/mol)	DANS calc frequency/cm^{-1}	mode description[b]
539			8	560	N−Me_2 scissors
749			14	745	amino ring def (12), sym N−Me_2 str
817			7	833	ring breathe (1), NO_2 scissors
874			42	867	NO_2 scissors, ring breathe (1)
962			22	1009	ethylenic out of plane H wag
1009			0.5	1024	ring defs (18a)
			3	1028	
1110	1108	1109, m	271	1134	C−NO_2 stretch
1167		1167, m	165	1210	sym Me in-plane rock
1188	1187	1188, m	8	1219	ring CH rocks (9a)
			252	1222	
	1204				paracyclophane
1322	1325		863	1373	sym NO_2 str + ethylenic H rock
1339	1342	1338, s	795	1387	sym NO_2 str + ethylenic H rock
1412		1412, vw	225	1407	C−N_{amino} str
1494			10	1541	nitro ring str (19a)
1556	1555	1554, w	272	1579	C−NMe_2 str + amino ring str (19a)
1585	1589	1583, s	963	1640	nitro ring "quinoidal" str (8a)
1610	1609	1608, m	231	1673	amino ring "quinoidal" str (8a)
1629	1625	≈1624, sh	9	1697	ethylenic C=C stretch

[a] Reference 41. [b] Notation for ring modes in parentheses is that of refs 13, 42, 46, and 49.

861, 1111, 1318, 1333, 1507, and 1601 cm^{-1}, respectively. Lines at 1009, 1167, 1412, 1556, and 1610 cm^{-1} correspond to NMe_2 and ring modes of DMABN at 1003, 1166, 1377, 1527, and 1606 cm^{-1}, respectively. The 1188 cm^{-1} band of DANS may contain the CH rocking 9a modes of both rings; this mode is assigned at 1179, 1179, and 1187 cm^{-1} in PNA, DMABN, and *trans*-stilbene, respectively. The 1629 cm^{-1} line of DANS is clearly the ethylenic C=C stretch found at 1639 cm^{-1} in *trans*-stilbene. The line at 962 cm^{-1}, which is seen in the dichloromethane solution but not in crystalline DANS, is assigned to an out-of-plane H wag of the olefinic linker. The A_u ethylenic H out-of-plane wag of *trans*-stilbene (963 cm^{-1}) exhibits an analogous intensity increase between crystal and solution phases attributed to distortions from planarity in solution.[47] A DFT normal-mode analysis was used to make plausible assignments for the 539 and 749 cm^{-1} vibrations and to support the empirical assignments. The calculated frequencies and infrared intensities are included in Table 2.

The only vibration of PCP−DANS that does not correspond to a similar mode in DANS is the one appearing at 1204 cm^{-1}. On the basis of AM1 results and a previous normal-mode analysis of PCP,[48] the 1204 cm^{-1} mode is likely to involve a C(aromatic)−C(aliphatic) stretch of the PCP core, although this assignment is by no means definitive. For the purposes of this work, it is most important to have solid assignments for the modes observed in both DANS and PCP−DANS.

IV. Discussion

The solvent dependence of the ground- and excited-state structures of push−pull molecules such as DANS is often discussed in the context of a two-state valence-bond model, as originally presented by Goddard and co-workers[50,51] and since extended by Blanchard-Desce et al.,[52,53] Thompson and Hynes,[54,55] and others.[56−58] In the notation of ref 55, the ground and excited electronic eigenstates Ψ_g and Ψ_e are expressed as linear combinations of neutral and zwitterionic diabatic basis states ψ_N and ψ_Z:

$$\Psi_g = (1 - f)^{1/2}\psi_N + f^{1/2}\psi_Z \quad (1a)$$

$$\Psi_e = -f^{1/2}\psi_N + (1 - f)^{1/2}\psi_Z \quad (1b)$$

where f, the fractional zwitterionic character in the ground state, is a function of the relative energies of ψ_N and ψ_Z as well as the electronic coupling between them. The basis states ψ_N and ψ_Z are taken to be orthogonal,[51,52] although this should not obviously be the case for structures such as those shown in Figure 1. In terms of this definition of the electronic states, the two-state valence-bond theory is identical to the Mulliken model for charge-transfer transitions, in which neutral (D−A) and charge-transfer (D^+-A^-) basis states are mixed through an electronic coupling to produce two electronic eigenstates, the ground state generally being predominantly neutral and the excited state predominantly charge-transfer in character.[59] The main difference is that the Mulliken model is usually applied to noncovalent or at least nonconjugated systems where the assumption of orthogonality between neutral and charge-transfer basis states is quite good. In push−pull systems where the neutral and zwitterionic basis states are resonance forms connected by a reversal of conjugated bond order alternation, the electronic coupling is much stronger and an appropriate definition of ψ_N and ψ_Z becomes trickier. This issue is discussed in some detail in ref 55.

Any two-state model for the electronic structure predicts that as the two basis states are brought closer in energy (for example by changing the solvent), the electronic eigenstates will also become closer in energy (the transition will red-shift) and the magnitudes of the basis-state coefficients in the two eigenstates will become more comparable (the electron densities in the two states will become more similar). Therefore, red-shifting the absorption should cause the ground and excited states to become more similar in structure, with an accompanying reduction in the internal vibrational reorganization. The two other push−pull chromophores with oxygen-containing accepting groups that we have studied (PNA and JTB) generally follow these qualitative expectations: as the solvent polarity increases, the absorption spectrum red-shifts and the internal vibrational reorganization energies decrease.[13,14] The exception is methanol, which exhibits an unusually large reorganization energy tentatively attributed to specific hydrogen-bonding interactions.[13,14] DANS could not be studied in nonpolar or weakly polar solvents because of strong interfering fluorescence, but the reduction in vibrational reorganization energy between dichloromethane and acetonitrile and the increase in λ_v in methanol are consistent

with the results obtained for the other molecules studied. In addition, the classical reorganization energy (arising mainly from solvent motions) is expected to increase in solvents of greater polarity because of the orientational component of the solvent polarization. DANS, PNA, and JTB all follow this trend except in methanol, which exhibits an anomalously low classical reorganization energy. This has been attributed to the slower time scale of solvent reorganization in a strongly hydrogen-bonded solvent,[13,14] as motions that are slow compared with ground-state vibrational dephasing contribute to inhomogeneous rather than homogeneous electronic spectral broadening in the resonance Raman analysis.

Although PCP−DANS was not investigated in multiple solvents, previous work has revealed interesting properties of the solvent-dependent emission in both molecules. Both DANS[33−36] and PCP−DANS[11] exhibit a significant decrease in fluorescence quantum yield in increasingly polar solvents. In the case of DANS, a quenching mechanism has been proposed which involves internal conversion to a nonradiative state characterized by a twisting of the nitro group.[35] The NO_2 twisting mode could not be observed in our experiments because it is too low in frequency (calculated at 62 cm^{-1}). The Stokes shifts of PCP−DANS exceed those of DANS by factors of 1.5 and 2.5 in cyclohexane and benzene, respectively, whereas in dimethylformamide the Stokes shift is slightly larger in DANS than in PCP−DANS.[11,35] However, in the case of PCP−DANS there are clearly either two emitting states or two conformations in very polar solvents,[11] so a direct comparison of Stokes shifts may not be meaningful. If the data in acetonitrile are representative, the partitioning of the excited-state reorganization is significantly different in the two species. The reorganization energies in Table 1 suggest that the internal contribution comprises a greater fraction of the total reorganization energy in DANS than in PCP−DANS.

The mode-specific contributions to the internal reorganization indicate further differences between the two molecules. As mentioned above, eight of the nine observed modes in PCP−DANS correspond to similar vibrations in DANS. The four observed modes localized mainly on the C−NO_2 parts of the structures (DANS frequencies 1110, 1322, 1339, and 1585 cm^{-1}) have significantly larger displacements in DANS than do the corresponding modes in PCP−DANS, especially the NO_2 stretch (see Table 2). The two modes localized on the C−NMe_2 parts of the structures (DANS frequencies 1556 and 1610 cm^{-1}) have smaller displacements in DANS than in PCP−DANS. The total reorganization energy in the five nitro ring localized vibrations of DANS (1110, 1322, 1339, 1494, and 1585 cm^{-1}) is 1775 cm^{-1}, while the corresponding total for the four observed nitro ring modes of PCP−DANS (1108, 1325, 1342, and 1589 cm^{-1}) is only 418 cm^{-1}. At the same time, the total reorganization energy in the four amino ring localized modes of DANS (1167, 1412, 1556, and 1610 cm^{-1}) is 158 cm^{-1}, while the corresponding total for the two amino ring localized modes of PCP−DANS (1555 and 1609 cm^{-1}) is 189 cm^{-1}. Thus, we infer that upon excitation a greater change in geometry takes place in the vicinity of the nitro acceptor group in DANS than in PCP−DANS, while the two molecules undergo similar and smaller geometry changes about the dialkylamino donor end.

To explain the relative displacements between DANS and PCP−DANS, it is necessary to consider the effect the PCP moiety has on the electronic structure. ZINDO calculations predict that the lowest strongly allowed transition in DANS is dominated by the HOMO ⟹ LUMO configuration. In contrast, ZINDO calculations on PCP−DANS predict nearly equal

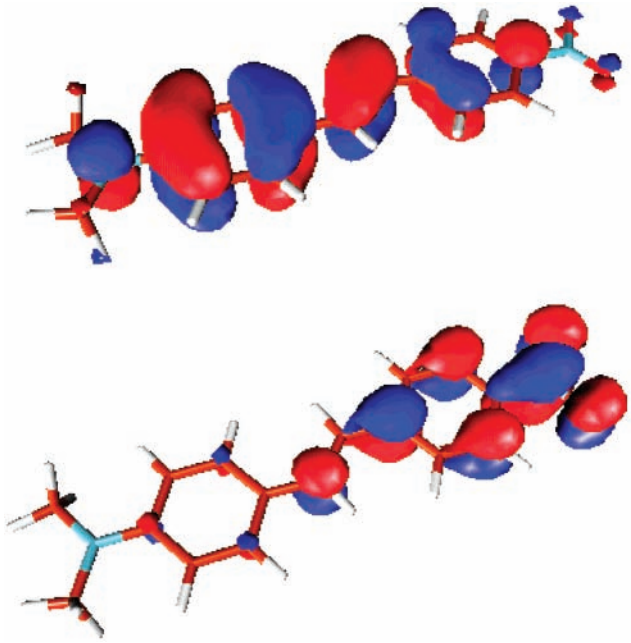

Figure 11. (top) HOMO and (bottom) LUMO of DANS. Both are plotted at a contour of 0.025 electrons/$bohr^3$.

contributions of the HOMO ⟹ LUMO and HOMO ⟹ LUMO + 2 configurations to the strongly allowed excited state. Figure 11 shows the HOMO and LUMO of DANS, whereas Figure 12 presents the HOMO, LUMO, and LUMO + 2 of PCP−DANS. The HOMO is localized on the donor end of the molecule and the LUMO is localized on the acceptor end of the molecule in both cases. However, the HOMO of DANS has significant amplitudes on both halves of the structure, whereas the HOMO of PCP−DANS has very little amplitude in the vicinity of the acceptor. The LUMO + 2 orbital of PCP−DANS (Figure 12c) has significant amplitudes on both ends of the molecule.

Examination of Figures 11 and 12 provides a qualitative rationalization for the differences in the excited-state displacements between DANS and PCP−DANS. In both molecules, the dominant contributions to the strongly allowed electronic excitation involve removing an electron from the HOMO, which has the greatest amplitudes on the donor ends of both molecules. However, the transition density of PCP−DANS is equally divided between configurations, whereas that of DANS is dominated by a single configuration (HOMO ⟹ LUMO). In both molecules the LUMO is localized around the nitro group, but in PCP−DANS the electronic excitation also has significant contributions from the delocalized LUMO + 2, resulting in smaller geometry changes around the nitro end of this molecule.

A detailed spectroscopic and computational study of the PCP−DANS analogue lacking the electron donor and acceptor groups (−NO_2 and −$N(hex)_2$ replaced by hydrogen atoms) has already been reported.[60] Calculations using the collective electronic oscillators (CEO) method with the INDO/S Hamiltonian predict that the two lowest singlet excited states are largely PCP-localized transitions, about 0.8 eV lower in energy than the stilbene-localized transitions. This prediction is consistent with the observation that the radiative rate for the emitting state(s) is about an order of magnitude lower than that of *trans*-stilbene itself. CEO calculations on PCP−DANS similarly predict two weak, PCP-localized transitions, 0.2−0.4 eV below the strongly allowed one.[61] The electronic structure calculations support the idea that the low-energy absorption band of PCP−DANS has contributions from more than one electronic state

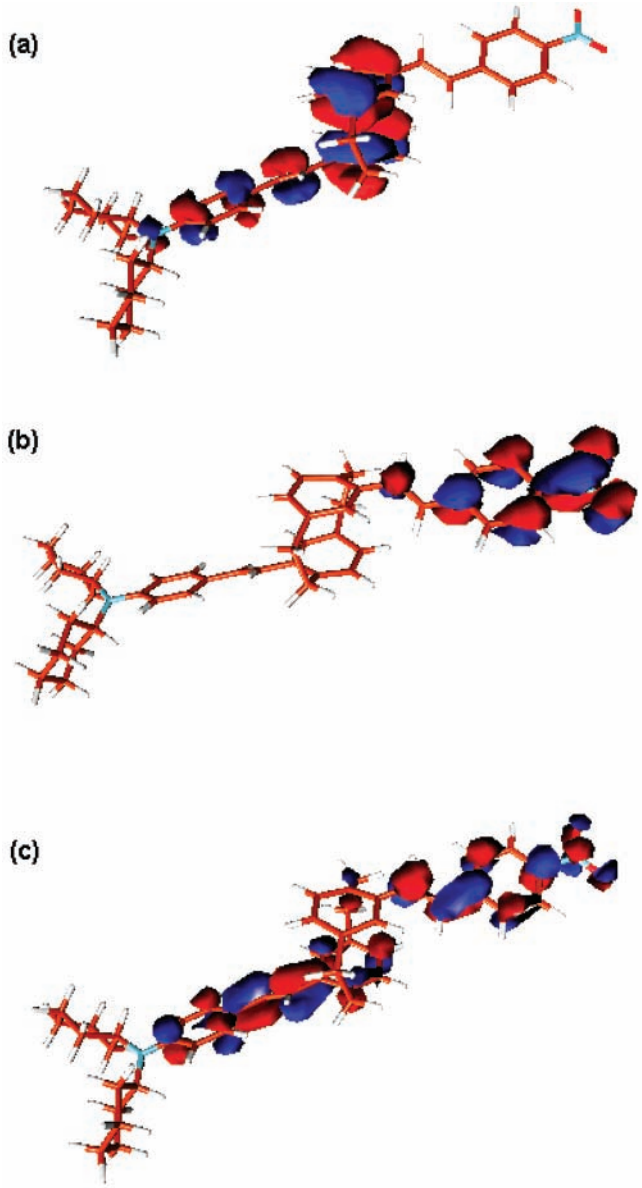

Figure 12. (top) HOMO, (middle) LUMO, and (bottom) LUMO + 2 of PCP−DANS. All are plotted at a contour of 0.025 electrons/bohr^3.

(ICT-like and PCP-localized) and/or that the transition giving rise to most of the oscillator strength in this region has a significant contribution from PCP-localized configurations.

The mode-specific reorganization energies of DANS can be compared to those of *p*-nitroaniline (PNA).[13] PNA has resonance-enhanced modes which are closely related to those of DANS at 1112, 1316, and 1322 cm^{-1}. The reorganization energies for these three modes of PNA are smaller than those of DANS. As in the case of DANS, the excited-state reorganization of PNA is greatest in the vicinity of the NO_2 group. The normal-mode displacements of the 1110 cm^{-1} C−NO_2 stretch and 1316/1322 cm^{-1} symmetric NO_2 stretch (the doublet was integrated as a single band because of overlap) in PNA are 0.242 and 0.976, respectively.[13] In the context of a two-state valence-bond model, the ground electronic eigenstate is composed primarily of the neutral basis state which is represented by a resonance form with zero formal charges on the donor and acceptor groups (Figure 1), whereas the excited electronic state is predominantly described by the zwitterionic basis state which is represented by a resonance form with nonzero formal charges on the donor (+1) and acceptor groups (−1). Relative to the distance in PNA, the calculated distance between the amino nitrogen and the midpoint between the two oxygen atoms is 2.1 times greater in DANS. Therefore, if the ground states of these molecules have equivalent basis-state compositions, the dipole moment of DANS should be roughly a factor of 2.1 times that of PNA. The dipole moment of PNA has been reported for a wide variety of solvents, and the values range from 6.1 to 7.8,[62] while the dipole moment of DANS in benzene[63] has been measured as 7.42 D. The nearly equal ground-state dipoles of DANS and PNA suggest that the ground electronic state of PNA is characterized by a larger zwitterionic contribution than that of DANS, which would imply that the ICT state of DANS must have a larger zwitterionic contribution than that of the ICT state of PNA. Therefore, the ICT transition of DANS is more "pure", in the sense that it is more properly described by the movement of an electron from the vicinity of the amino nitrogen to the acceptor group, than is the excitation in PNA. It follows that the excitation in DANS involves a larger change in charge density in the vicinity of the donor and acceptor groups and therefore that DANS undergoes larger geometry changes in these regions than does PNA. Previous work has suggested that the two-state valence-bond model cannot quantitatively account for the solvent dependence of the ground- and excited-state structures,[13,14,40] but the predicted qualitative trends appear to be followed.

V. Conclusions

Resonance Raman intensity analysis of nominally charge-transfer electronic transitions in DANS and PCP−DANS reveals differences in the nature of the excited electronic states in the two molecules. The transition in DANS displays characteristics of a typical intramolecular charge-transfer transition, whereas the transition in PCP−DANS is less charge-transfer-like in nature. The mode-specific reorganization energies obtained from the spectroscopic modeling indicate that electronic excitation produces a significantly larger geometry change in the vicinity of the nitro acceptor group in DANS relative to PCP−DANS, while the geometry changes in the vicinity of the dialkylamino group are comparable for the two molecules. These results are interpreted with the aid of semiempirical (ZINDO) predictions of excited-state compositions. These calculations confirm a dominant charge-transfer character in the case of DANS, whereas the corresponding calculations for PCP−DANS predict a significant contribution from configurations localized on the PCP moiety.

Acknowledgment. This work was supported by ACF-PRF Grant 33963-AC6 and NSF Grant CHE-0109920. We thank Dr. Sergei Tretiak for the X-ray coordinates of the PCP core and for the CEO calculations on PCP−DANS, and Gustavo Seabra for assistance with the ZINDO calculations.

References and Notes

(1) Marder, S. R.; Beratan, D. N.; Cheng, L.-T. *Science* **1991**, *252*, 103−106.

(2) Prasad, N. P.; Williams, D. J. *Introduction to Nonlinear Optical Effects in Molecules and Polymers*; Wiley: New York, 1991.

(3) *Molecular Nonlinear Optics: Materials, Physics, and Devices*; Zyss, J., Ed.; Academic Press: Boston, 1993.

(4) Kanis, D. R.; Ratner, M. A.; Marks, T. J. *Chem. Rev.* **1994**, *94*, 195−242.

(5) Marder, S. R.; Cheng, L.-T.; Tiemann, B. G.; Friedli, A. C.; Blanchard-Desce, M.; Perry, J. W.; Skindhøj, J. *Science* **1994**, *263*, 511−514.

(6) Lu, D.; Marten, B.; Cao, Y.; Ringnalda, M. N.; Friesner, R. A.; Goddard, W. A., III. *Chem. Phys. Lett.* **1995**, *242*, 543−547.

(7) Albert, I. D. L.; Marks, T. L.; Ratner, M. A. *J. Phys. Chem.* **1996**, *100*, 9714−9725.
(8) Shu, Y.-C.; Gong, Z.-H.; Shu, C.-F.; Breitung, E. M.; McMahon, R. J.; Lee, G.-H.; Jen, A. K.-Y. *Chem. Mater.* **1999**, *11*, 1628−1632.
(9) Thayumanavan, S.; Mendez, J.; Marder, S. R. *J. Org. Chem.* **1999**, *64*, 4289−4297.
(10) Rojo, G.; Agulló-López, F.; Cabezón, B.; Torres, T.; Brasselet, S.; Ledoux, I.; Zyss, J. *J. Phys. Chem. B* **2000**, *104*, 4295−4299.
(11) Zyss, J.; Ledoux, I.; Volkov, S.; Chernyak, V.; Mukamel, S.; Bartholomew, G. P.; Bazan, G. C. *J. Am. Chem. Soc.* **2000**, *122*, 11956−11962.
(12) Ma, H.; Chen, B.; Sassa, T.; Dalton, L. R.; Jen, A. K.-Y. *J. Am. Chem. Soc.* **2001**, *123*, 986−987.
(13) Moran, A. M.; Kelley, A. M. *J. Chem. Phys.* **2001**, *115*, 912−924.
(14) Moran, A. M.; Delbecque, C.; Kelley, A. M. *J. Phys. Chem. A* **2001**, *105*, 10208−10219.
(15) Lilichenko, M.; Tittelbach-Helmrich, D.; Verhoeven, J. W.; Gould, I. R.; Myers, A. B. *J. Chem. Phys.* **1998**, *109*, 10958−10969.
(16) Hupp, J. T.; Williams, R. D. *Acc. Chem. Res.* **2001**, *34*, 808−817.
(17) McHale, J. L. *Acc. Chem. Res.* **2001**, *34*, 265−272.
(18) Fraga, E.; Loppnow, G. R. *J. Phys. Chem. B* **1998**, *102*, 7659−7665.
(19) Kwok, W. M.; Phillips, D. L.; Yeung, P. K.-Y.; Yam, V. W.-W. *J. Phys. Chem. A* **1997**, *101*, 9286−9295.
(20) Yamaguchi, T.; Kimura, Y.; Hirota, N. *J. Chem. Phys.* **1998**, *109*, 9075−9083.
(21) Gurzadyan, G.; Görner, H. *Chem. Phys. Lett.* **2000**, *319*, 164−172.
(22) Görner, H. *J. Photochem. Photobiol., A* **1987**, *40*, 325−339.
(23) Oldham, W. J., Jr.; Miao, Y.-J.; Lachicotte, R. J.; Bazan, G. C. *J. Am. Chem. Soc.* **1998**, *120*, 419−420.
(24) Myers, A. B. In *Laser Techniques in Chemistry*; Myers, A. B., Rizzo, T. R., Eds.; Wiley: New York, 1995; pp 325−384.
(25) Myers, A. B.; Li, B.; Ci, X. *J. Chem. Phys.* **1988**, *89*, 1876−1886.
(26) Markel, F.; Ferris, N. S.; Gould, I. R.; Myers, A. B. *J. Am. Chem. Soc.* **1992**, *114*, 6208−6219.
(27) Li, B.; Johnson, A. E.; Mukamel, S.; Myers, A. B. *J. Am. Chem. Soc.* **1994**, *116*, 11039−11047.
(28) Kulinowski, K.; Gould, I. R.; Myers, A. B. *J. Phys. Chem.* **1995**, *99*, 9017−9026.
(29) Zerner, M. C.; Loew, C. H.; Kirchner, R. F.; Mueller-Westerhoff, U. T. *J. Am. Chem. Soc.* **1980**, *102*, 589.
(30) Ridley, J.; Zerner, M. C. *Theor. Chim. Acta* **1973**, *32*, 111.
(31) Frisch, M. J.; Trucks, G. W.; Schlegel, H. B.; Scuseria, G. E.; Robb, M. A.; Cheeseman, J. R.; Zakrzewski, V. G.; Montgomery, J. A., Jr.; Stratmann, R. E.; Burant, J. C.; Dapprich, S.; Millam, J. M.; Daniels, A. D.; Kudin, K. N.; Strain, M. C.; Farkas, O.; Tomasi, J.; Barone, V.; Cossi, M.; Cammi, R.; Mennucci, B.; Pomelli, C.; Adamo, C.; Clifford, S.; Ochterski, J.; Petersson, G. A.; Ayala, P. Y.; Cui, Q.; Morokuma, K.; Malick, D. K.; Rabuck, A. D.; Raghavachari, K.; Foresman, J. B.; Cioslowski, J.; Ortiz, J. V.; Baboul, A. G.; Stefanov, B. B.; Liu, G.; Liashenko, A.; Piskorz, P.; Komaromi, I.; Gomperts, R.; Martin, R. L.; Fox, D. J.; Keith, T.; Al-Laham, M. A.; Peng, C. Y.; Nanayakkara, A.; Gonzalez, C.; Challacombe, M.; Gill, P. M. W.; Johnson, B.; Chen, W.; Wong, M. W.; Andres, J. L.; Gonzalez, C.; Head-Gordon, M.; Replogle, E. S.; Pople, J. A. *Gaussian 98*, revision A.7; Gaussian, Inc.: Pittsburgh, PA, 1998.
(32) Dewar, M. J. S.; Zoebisch, E. G.; Healy, E. F.; Stewart, J. J. P. *J. Am. Chem. Soc.* **1985**, *107*, 3902−3909.
(33) Shin, D. M.; Whitten, D. G. *J. Phys. Chem.* **1988**, *92*, 2943−2956.
(34) Gruen, H.; Görner, H. *J. Phys. Chem.* **1989**, *93*, 7144−7152.
(35) Lapouyade, R.; Kuhn, A.; Letard, J.-F.; Rettig, W. *Chem. Phys. Lett.* **1993**, *208*, 48−58.
(36) Jager, W. F.; Sarker, A. M.; Neckers, D. C. *Macromolecules* **1999**, *32*, 8791−8799.
(37) Stein, P.; Miskowski, V.; Woodruff, W. H.; Griffin, J. P.; Werner, K. G.; Gaber, B. P.; Spiro, T. G. *J. Chem. Phys.* **1976**, *64*, 2159−2167.
(38) Markel, F.; Myers, A. B. *J. Chem. Phys.* **1993**, *98*, 21−30.
(39) Bailey, S. E.; Cohan, J. S.; Zink, J. I. *J. Phys. Chem. B* **2000**, *104*, 10743−10749.
(40) Moran, A. M.; Egolf, D. S.; Blanchard-Desce, M.; Kelley, A. M. *J. Chem. Phys.* **2002**, *116*, 2542−2555.
(41) Okamoto, H.; Tasumi, M. *Chem. Phys. Lett.* **1996**, *256*, 502−508.
(42) Meic, Z.; Güsten, H. *Spectrochim. Acta, Part A* **1978**, *34*, 101−111.
(43) Gustafson, T. L.; Roberts, D. M.; Chernoff, D. A. *J. Chem. Phys.* **1983**, *79*, 1559−1564.
(44) Hamaguchi, H.; Kato, C.; Tasumi, M. *Chem. Phys. Lett.* **1983**, *100*, 3−7.
(45) Hamaguchi, H.; Okamoto, H.; Tasumi, M.; Mukai, Y.; Koyama, Y. *Chem. Phys. Lett.* **1984**, *107*, 355−359.
(46) Kwok, W. M.; Ma, C.; Matousek, P.; Parker, A. W.; Phillips, D.; Toner, W. T.; Towrie, M.; Umapathy, S. *J. Phys. Chem. A* **2001**, *105*, 984−990.
(47) Edelson, M.; Bree, A. *Chem. Phys. Lett.* **1976**, *41*, 562−564.
(48) Walden, S. E.; Glatzhofer, D. T. *J. Phys. Chem. A* **1997**, *101*, 8233−8241.
(49) Varsanyi, G. *Assignments for Vibrational Spectra of Seven Hundred Benzene Derivatives*; Wiley: New York, 1974.
(50) Chen, G.; Lu, D.; Goddard, W. A., III. *J. Chem. Phys.* **1994**, *101*, 5860−5864.
(51) Lu, D.; Chen, G.; Perry, J. W.; Goddard, W. A., III. *J. Am. Chem. Soc.* **1994**, *116*, 10679−10685.
(52) Barzoukas, M.; Runser, C.; Fort, A.; Blanchard-Desce, M. *Chem. Phys. Lett.* **1996**, *257*, 531−537.
(53) Blanchard-Desce, M.; Barzoukas, M. *J. Opt. Soc. Am. B* **1998**, *15*, 302−307.
(54) Thompson, W. H.; Blanchard-Desce, M.; Alain, V.; Muller, J.; Fort, A.; Barzoukas, M.; Hynes, J. T. *J. Phys. Chem. A* **1999**, *103*, 3766−3771.
(55) Thompson, W. H.; Blanchard-Desce, M.; Hynes, J. T. *J. Phys. Chem. A* **1998**, *102*, 7712−7722.
(56) Bishop, D. M.; Champagne, B.; Kirtman, B. *J. Chem. Phys.* **1998**, *109*, 9987−9994.
(57) Castiglioni, C.; Del Zoppo, M.; Zerbi, G. *Phys. Rev. B: Condens. Matter Mater. Phys.* **1996**, *53*, 13319−13325.
(58) Painelli, A.; Terenziani, F. *J. Phys. Chem. A* **2000**, *104*, 11041−11048.
(59) Mulliken, R. S.; Person, W. B. *Molecular Complexes*; Wiley-Interscience: New York, 1969.
(60) Bazan, G. C.; Oldham, W. J., Jr.; Lachicotte, R. J.; Tretiak, S.; Chernyak, V.; Mukamel, S. *J. Am. Chem. Soc.* **1998**, *120*, 9188−9204.
(61) Tretiak, S. Personal communication.
(62) Stähelin, M.; Burland, D. M.; Rice, J. E. *Chem. Phys. Lett.* **1992**, *191*, 245−250.
(63) Everard, K. B.; Kumar, L.; Sutton, L. E. *J. Chem. Soc.* **1951**, 2807.